Université Grenoble Alpes
PhITEM

Master thesis
Master Atmosphere Climate and Continental Surfaces

Study of seismic data from a dense array recorded on the Argentière Glacier

Benoît Urruty

Supervisors :
Florent Gimbert
Philippe Roux

4th February 2019 — 26th July 2019

UFR PhITEM

UNIVERSITÉ Grenoble Alpes

OSUG

Observatoire des Sciences de l'Univers de Grenoble

Master in Earth, planetary and Environmental Sciences

Non-plagiarism certificate

I, the undersigned (First name, FAMILY NAME)

Benoît URRUTY

Author of the report entitled (Title)

Study of the seismic data from a dense array recorded on the Argentière Glacier

Declare that the above-cited report results from my personal work and that I have neither forged, falsified nor copied all or part of another persons work to present it as mine.

All sources of information used and all author citations have been included following standard usage.

I am aware of the fact that failing to cite a source or failing to cite it fully and properly constitutes plagiarism, and that plagiarism is considered a serious offence within the university that can be sanctioned severely by law.

At (place) Saint Martin d'Hères,

the (date) 7/06/19

Student's signature

Abstract

To aim a better understanding of the glacier physics, we explore the Argentière glacier by seismic method. We used a dense array of sensors to provide a fine exploration of the glacier. The data was processed with Match Field Processing (MFP) which provides an enormous number of sources, 172798 per day and per frequency. This set up is unique and we define the best way to explore this data set. We select only the good located sources which correspond to the expected characteristics and location. We determine the limits of the method and the characteristics of the data as a function of frequency. We have really nice observations of the surface activity near the mesh. The sources are following crevasses and a velocity propagation and the seismicity rates are measured. On the whole surface, the seismicity rates are closely linked to the temperature. These phenomena are related to the physics of the glacier. We establish a relation between propagation velocity and crack propagation, while the seismicity rates seem to be linked to cold temperature.

Résumé

Dans le but de mieux comprendre la physique des glaciers, nous explorons le glacier d'Argentière par la sismique. Nous avons utilisé un réseau dense de capteurs pour permettre une exploration fine du glacier. Les données ont été traitées par un algorithme de Match Field Processing (MFP), qui fournit un nombre élevé de sources relocalisées, 172798 par jour et par fréquence. Cette configuration est unique et nous définissons le meilleur moyen d'explorer cet ensemble de données. Nous sélectionnons uniquement les sources bien localisées qui correspondent aux caractéristiques et à l'emplacement attendus. Nous déterminons les limites de la méthode et les caractéristiques des données en fonction de la fréquence. Nous avons de belles observations de l'activité de la surface près du maillage. Les sources suivent les zones crevasses. Sur ces zones, une vitesse de propagation ainsi que des taux de sismicité sont mesurés. Sur l'ensemble de la surface, les taux de sismicité sont étroitement liés à la température. Ces phénomènes liés à la physique du glacier nous permettent de lier la vitesse de propagation et la propagation des failles dans la glace, tandis la sismicité semble être liée aux températures froides.

Acknowledgement

This internship was a great experience and adventure, from the discovery of this data to the nice observations passing by the field work.

I would like to thank my supervisors Florent and Philippe who guided me across all the difficulties I encountered. They helped me to provide the work you will read.

Thanks to the RESOLVE team, they included me in the project. We had a great time to work together. I had to work with all of them personally. I compared my results with Agnès Helmstetter and Ugo Nanni, they helped me to confirm my results and to progress in my exploration of the data. Stéphane Garambois help me to use the software geopsy, which is useful to invert a dispersion curve.

I would like to thank Fabian Walter for accepting to be the reporter of my work.

Thanks to my reviewers: my supervisors, Arya Gorgy, Solveig Raymond, Jacques Brives, and my brother Thierry

Contents

1 Introduction

Glaciers and ice-caps represent 70% of freshwater storage on Earth. Global warming is stronger in mountain regions, with temperatures increasing twice faster than the global average (Pepin et al., 2015). This rapid rate of temperature rise has a severe effect on glaciers. Thus, the understanding of glacier mechanisms is a real challenge, with global warming driving rapid change in both meteorology and glacier evolution in the coming decades. First, glaciers are the main contributors to rising sea levels (Vaughan et al., 2013)(Bamber et al., 2018). These rapid changes also have a serious effect on populations. Glaciers represent freshwater supply (Huss et al., 2014) for many cities in the world such as La Paz (Bolivia) (Soruco et al., 2015). However, they can also be threats for populations, such as for example outbursts and floods induced by the sudden drainage of pro- and sus-glacial lakes, *e.g.* in Tête Rousse glacier (Vincent et al., 2010)(Vincent et al., 2012). Physical mechanisms occurring at the base of the glacier and the crevasse formation are poorly understood, and therefore related to many discussions and studies. The limiting factor is that access to the bottom of a glacier is complicated (Walter et al., 2013). The impact of crevasses structures in the glacier mass balance is reported many times (Colgan et al., 2016) but their propagation and formation remain poorly documented.

Alpine glaciers are well monitored. Their length (Vincent et al., 2009), mass balance (Gerbaux et al., 2005) and velocity field (Rabatel et al., 2018) are commonly characterized. Each year, the GLACIOCLIM team (https://glacioclim.osug.fr/spip.php?lang=en) follows these ice bodies to provide the evolution state of the glaciers in the Alps, the Andes and Himalaya. In the Alps, the first scientific observation of a glacier dates back to 1905. Nowadays, most of the alpine glaciers have been described by remote sensing (Rabatel et al., 2005). It's a method which provides pictures of the glacier by satellite but within a period of few tens of days. Observations have been made in the surface. Precise characterization of the crevasse as a fault propagation is not described. The results of this report will address this issue.

The RESOLVE project aims to better understand basal sliding, glaciers fracturing and the subglacial hydrology (RESOLVE, 2017) from fine geophysical observations. It gathers the Institut des Geosciences de l'Environnment (IGE) and the Institut des Sciences de la Terre (ISTerre) both laboratories in which I am currently doing this internship. The project is unique in the number of sensors deployed and the duration of the acquisition. The acquisition was done in spring 2018 on the Argentière Glacier. The project is based on results obtained from an array of 98 seismic sensors placed on the glacier.

In geophysics, passive seismology methods are used to characterize a medium using the surrounding wavefield, which is mainly composed by ambient noise and impulsive sources. The ambient noise is composed by the continuous noise from hydrology, wind and human activities. The impulsive sources are icequakes, earthquakes or active human sources (explosive, hammer,...). Nowadays, thanks to the development of new sensors, it is getting more and more common to set a dense array of seismometers. This method is now extensively used for seismic tomography and monitoring which particularly benefit from the development of dense array. Actually, this type of setting provides better detection of small earthquakes and anthropogenic noise (Gradon et al., 2019) and can also be applied to rivers in the case of turbulent flows for the study of the bedload (Gimbert et al., 2014). The use of such a dense seismic array on a glacier like in Argentière has never been made before. The application of a method, used

for fifteen years on earth, on the glacier provides a rare opportunity to observe unknown sources and to characterize them. We expect to detect icequake from the bed sliding (Helmstetter et al., 2015), the subglacial hydrology (Fountain and Walder, 1998) and the propagation and geometry of crevasses (Preiswerk et al., 2018).

The past decade has seen the rapid development of cryoseismology in many studies (Podolskiy and Walter, 2016) . Many of the glacier structures such as caving and crevasses are monitored and characterized in terms of frequency and magnitude domains. These events covered a width range of frequencies from 10^{-3} to 10^{2} Hz (Podolskiy and Walter, 2016). The methods used in this field are passive, which means we are recording the wavefield propagating through the glacier. The glacier is producing icequakes which are a brittle deformation of the ice (Walter et al., 2013) and is producing impulsive signal. Since the instrumentation is easier to set up in isolated sites, studies have been done on the Greenland (Sergeant et al., 2019) and Antarctica ice-sheet, but also on mountain glaciers as Aletschgletscher (Preiswerk and Walter, 2018). The processes behind seismic sources on mountain glaciers are provided by crevasses extension and formation, subglacial water flows and stick-lip motions (Larose et al., 2015). Seismic methods are also used to study calving, (Sergeant et al., 2019)(Richardson et al., 2010) which is the release of ice chunks from the edge of a glacier, on ice-shelfs and to determine the volume of the calving iceberg. Podolskiy et al. (2018) were even able to describe diurnal variations as thermal fracturing but they could not locate the source.

The seismic data from the 98 seismic nodes of the RESOLVE project have first been pre-processed by a beamforming algorithm which allows to locate sources. This type of data set is pretty new for a glacier and we expect to find sources from the hydrological system and basal sliding. Basal icequakes have already been reported on this glacier as shown in Helmstetter et al. (2015), they were determined by S and P waves. We explore the whole data set with different methods in order to extract the most results from it.

In the following report, we investigate in detail the diversity of events observed from dense seismic array as well as their spatio-temporal characteristic. We do not have any a priori on the sources type. This report will first describe the study area, the instrumentation and the pre-processing of the seismic data. In a second part, the methods and the processing we apply to the data will be explained. Next, the results will be described. Finally, the observed glacier structures and content of the recorded wave-field will be discussed.

2 Study field and instrumentation

2.1 Argentière Glacier and long term instrumentation

The Argentière glacier is located in the Mont-Blanc massif in the French Alps. It extends on 10 km from 3400 m above sea level (asl) to the tongue at 1600 m asl with an average thickness of 200m. This glacier is monitored every year for the mass balance, velocity field and length variations. In 2013 ,its average speed was around 55m/yr(Vincent and Moreau, 2016) and mass balance was negative around $-1 mw.e.a^{-1}$ (meter water equivalent per year) (Vincent et al., 2009). These data are available on the GLACIOCLIM database. Our interest zone is between 2300 m and 2400 m asl, it was chosen because

it is on the ablation part and there are not too many crevasses there. The thickness of this field is around 200 m (Rabatel et al., 2018).

A meteorological station is long-term installed on the side of the Glacier (fig. 1) and is providing temperature, wind velocity and precipitations with a frequency of measurement of 30 minutes.

Under the glacier, Emosson S.A., a company producing hydroelectricity, is captures water under the glacier to drive it to the hydroelectric power station. They have access to cavities beneath the Lognan icefall (fig. 1). A cavitometer (bike wheel) was installed in 1970 to measure the basal sliding velocity of the glacier (Vivian and Bocquet, 1973). This unique instrument was improved in 2017 to an hourly frequency measurement. Emosson S.A. is providing the discharge measurement of their water catchment with a frequency of a quarter of hour from mid-spring to early autumn with an accuracy of 0.0109 m^3/s. This measurement is done by means of an Endress Hauser sensor measuring the water level in a calibrated channel. The water discharge range of measurements is limited by the accuracy of the measurement as a minimum and by the Emosson legislation limit at 10 m^3/s as a maximum. The sediments are collected and when it's full they drain them. Flushes are recorded and cause spikes in the discharge record (Vincent and Moreau, 2016).

2.2 Instrumentation of the RESOLVE Project

A multitude of geophysical instruments were deployed for the RESOLVE project, see on figure 1. All of these measurements provide a large data set. A precise elevation model of the surface was done in September 2018 and is useful to locate this data. The GPR (ground-penetrating radar) tracks provide us the bedrock elevation model and then the thickness of the glacier.

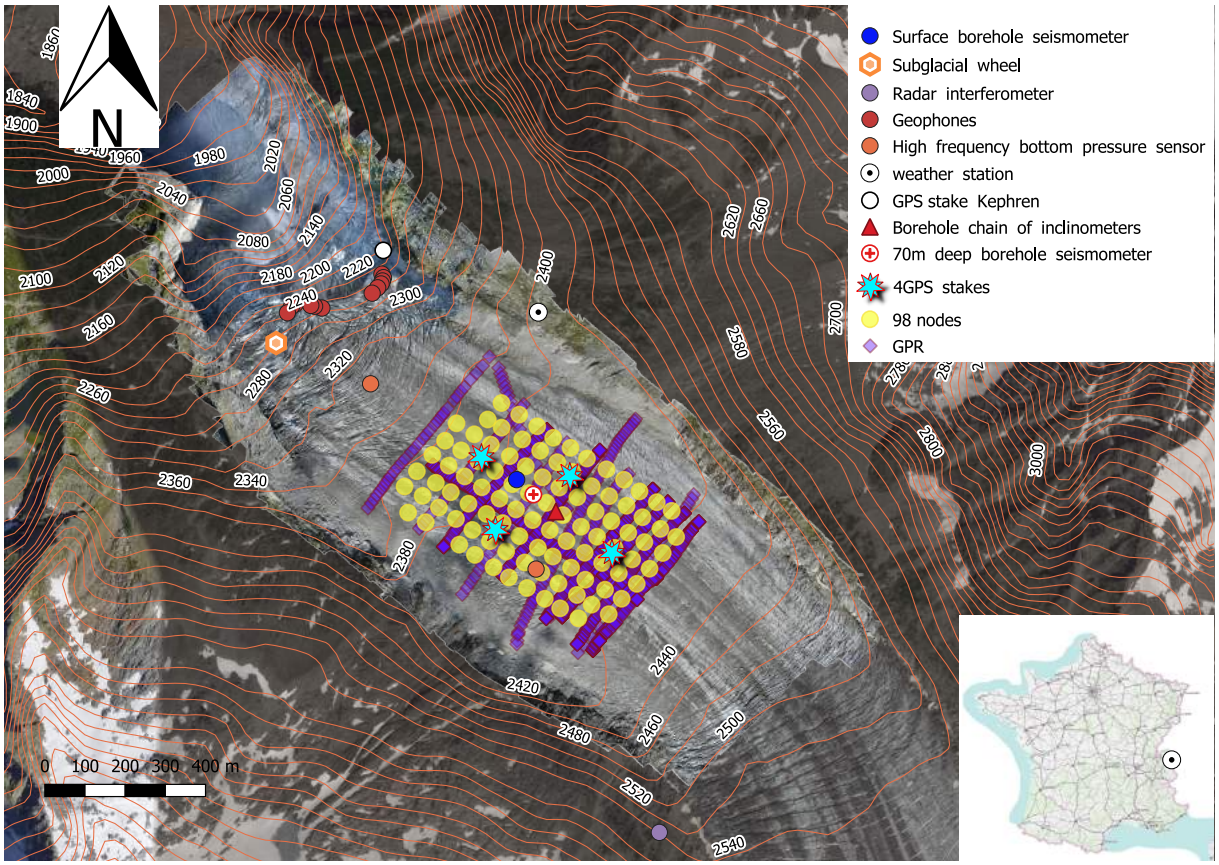

Figure 1: Presentation and location of the instruments on the Argentière glacier

We focus on the seismic data from the nodes mesh (see yellow dots in Figure 1). The seismic sensors are Fairfield ZLand 3C nodes (fig. 2) set up with a sampling frequency of 400 Hz. The sensors have a cut-off frequency of 4,5Hz. They were placed 40m apart from each other. They have a lifespan of 35 days. Each node was installed vertically.

Figure 2: Picture of a seismic node overturned after melting of the snow. credit: Ugo Nanni

The nodes mesh was set up from the 24^{th} of April to the 2^{d} of June 2019. There are some gaps in the data because the nodes switched them off. The reasons of their interruption can be that their verticality is wrongly adjusted ,or that some nodes ran out of power at the end of the experimentation. We focus on data from the 25^{th} April to the 26^{th} of May to make use of the best part of the data.

A dense array of sensors of this duration has never been done on glaciers before. This type of data is unique and we can expect lots of results from them.

3 Methods and Data Processing

These types of data have never been used before. A way to explore a 5-D matrix has to be determined in order to have only the exploitable results.

3.1 Signal Processing : the beamforming

We want to locate all types of sources detected by the array of sensors. We use an algorithm using the phase coherence across the array and locate for each time step.

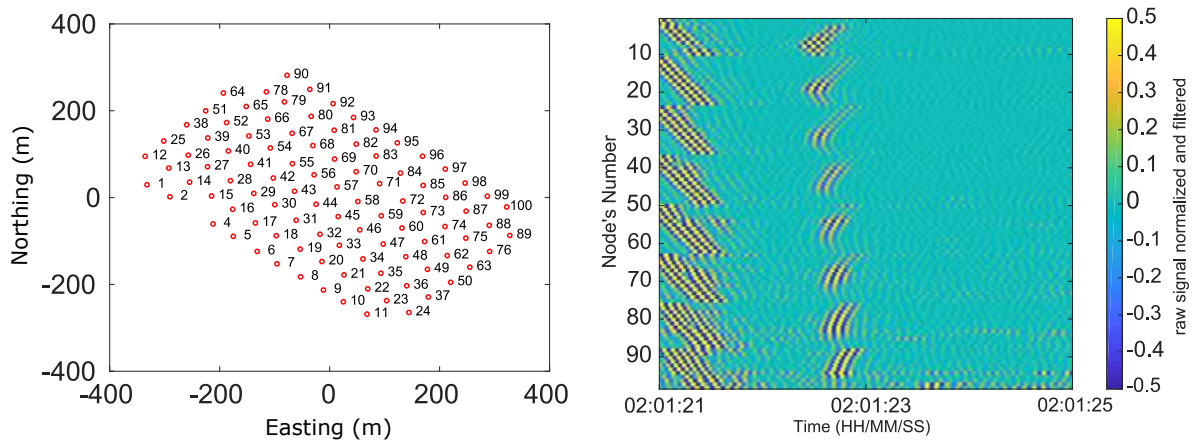

(a) (b)

Figure 3: (a) : Geometry of the nodes mesh with the number related to each node. (b) : Raw signal recorded between 10 and 16 Hz by the 98 nodes (Y axis) during a period of 4 seconds (X axis). The colors correspond to the normalized amplitude of the signal.

The algorithm described below have been performed and run by Albanne Lecointre (ISTerre).

The raw signal (fig. 3b) is recorded by the 98 nodes (fig. 3a). We are looking inside it for phase coherence. On figure 3b, we observe to period of phase coherence. The first one from the second 21 to $21,5$. The first sensors to receive the signal are the ones of the North-East of the set-up. A second phase coherence is observable from the seconds $22,5$ to 23 . The shape of the arriving signal is curvy. All the signal was processed by Match field processing (MFP) which is a type of beamforming algorithms. The goal of this algorithm is to recognize the phase coherence and to use it to located the origin of this signal. This signal is first filtered in a range of frequencies $\pm$3Hz around a given frequency. The algorithm is using central frequency from 5 Hz to 31 Hz with a step of 0,5Hz. The MFP algorithm is processed by the correlation between each node to compute the time lag of the signal. We define 11 starting points from which the algorithm will start the location of a source. The location is found when the Bartlett processor is maximum. The Bartlett operator is defined by $B(a,\omega)_{normalized} = \frac{\sum_\omega |b^*(a,\omega) \cdot K(\omega) \cdot b(a,\omega)|}{N^2}$

Where :

- $b(\omega, a) = A_j(\omega, a)e^{i\omega t_j(a)}$ the replica computed with A_j the amplitude term, ω the angular frequency, a =[X V] the parameters, X the source coordinate, V the medium velocity (to be inverted) and $t_j(a)$ the travel time. It's similar to the Green's function.
- $K(\omega) = d^*(\omega) \cdot d(\omega)$ the cross spectral density matrix (CSDM) with $d(\omega)$ a complex vector from the Fourier transform of windowed time series
- N the number of sensors

The Bartlett operator is a robust and stable optimal solution based on the phase of the signal (Gradon et al., 2019). The maximum value of this output 1 means a perfect correlation between the signal, and the minimum can be close to 0 meaning a total absence of correlation.

X	Y	Z	C	Beam
544.987182617188	-126.150840759277	-1421.15686035156	3311.83325195312	0.623493850231171
-8232.771484375	1966.95849609375	-68696.984375	78131.0546875	0.603587797927856
-8695.736328125	-4402.87158203125	-3194.03735351562	309421.59375	0.540538907051086
-2103.384765625	-23863.94140625	-56213.0390625	48153.30859375	0.563297808170319
47771.01171875	-43722.79296875	-337025.125	198776.921875	0.618947207927704
-13041.1259765625	17605.685546875	-43781.234375	81044.9921875	0.643018245697021
20411.9375	6109.2421875	-59357.99609375	26222.4453125	0.563912510871887
675.414245605469	-19252.484375	-35579.84765625	33358.7890625	0.65171492099762
3947.75512695312	-6528.07373046875	-35552.78515625	12977.1826171875	0.641904234886169
-14577.470703125	1353.66345214844	-9716.447265625	75461.34375	0.614630818367004

Figure 4: example of the 5-D matrix with the 5 variables of a located source. XYZ in m. C in m/s. Beam is the beamformer output.

The computation of the beamformer makes it possible to obtain a source location for a given time step, a half second in our case. The output of this computation is a 5-D matrix. For each source, we have the position in XYZ as well as the propagation speed of the wave and the Bartlett value (fig. 4). When the signal is noisy because of the ambient noise or a large number of sources, the correlation value decreases. The beamforming algorithm allows to locate only one source on a time step (0.5s). Relocation can be biased or erroneous for low beamforming values. It's meaning that the calculation takes into account multiple sources at once or noise.So, it's does not obtained a good coherence of phase of the signal, and it results in a low Bartlett.

The number of sources located is 172798 per day for each frequency but we choose only a part of them. In the case, we choose the sources at every frequency with a beamformer output higher than 0,5 and no other restrictions, we have more than 2×10^5 events per day and sometimes more than a million. We are making choice as a function of their location (XYZ) and their characteristic (C and the output). In order to look for sources with a good location (output higher than 0.5), we keep around 1×10^5 events per frequency on the 32 days of experimentation (fig. 5b).

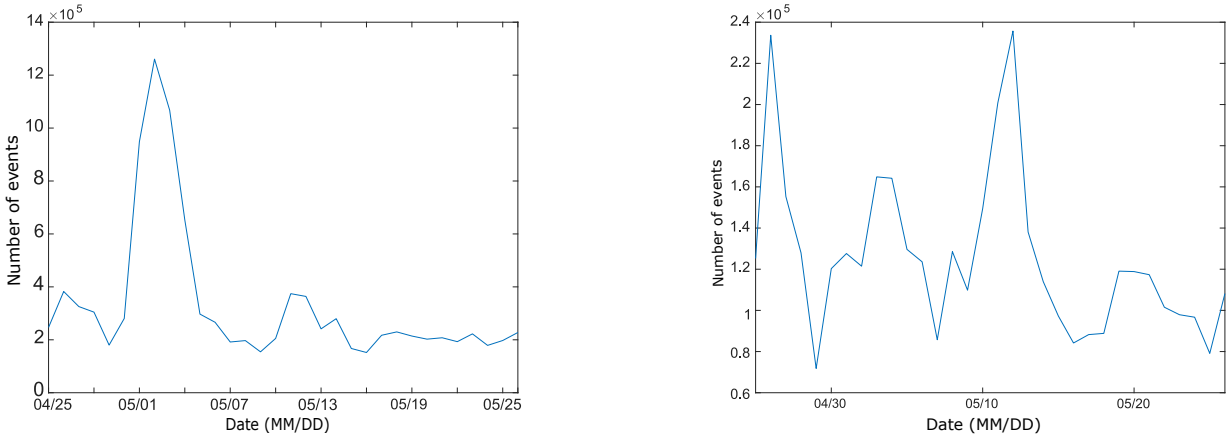

(a) (b)

Figure 5: Curve showing the number of events per day (a) : Number of sources per day with a beamformer output higher than 0,5 with no other choices of the parameters. (b) : Number of sources per day for a beamformer output higher than 0,5 inside the mesh and with a selected propagation propagation.

3.2 Choice of the frequency

The choice of frequency is dependant on the sensors and the distance between the nodes. As we said before, the sensors are limited by the cut off frequency at 4,5Hz. The observable frequency are limited by $\Delta x < \frac{v}{2f}$ where Δx is the distance between the sensors, v the velocity of the S-waves in the media and f their frequency. This equation means that in this configuration with all the sensors spreed by at least 40m, the maximum frequency f is at 20Hz. In this case, we have mainly surface waves with a speed around 1600m/s (Aster and Winberry, 2017). High frequencies have a short wave-length and are more rapidly attenuated by the medium. When we increase the frequency, the maximal distance between the mesh and the source reduces because of the attenuation. The attenuation is defined as $A(x) = A_0 e^{-\frac{pifx}{V_c Q}}$ where A_0 is the initial amplitude, f the frequency, x the distance to the source, V_c the velocity and Q the attenuation factor. It's the same effect with depth. If we want deep sources, we need to use low frequency but for the surface we can use higher. We choose the frequency as a function of what we look for. We know from Podolskiy and Walter (2016) the range of frequency of the different events which are occurring on a glacier. The anthropogenic and hydrological noise are mainly around 5Hzas describe for the hydrological noise in Gimbert et al. (2016).

3.3 Choice of the threshold T_B and quantification of uncertainties

It's therefore necessary to choose a threshold on the beamformer output to keep only "well" located sources. For each frequency, the distribution of this correlation value is different (fig. 6).

From this distribution, we can output for each frequency a minimum threshold value that allows us to have unbiased sources. We choose first to take the curve on figure 6b as the threshold chosen for each frequency. This curve is define by all the peak on fig. 6a. We use all sources from the eleven starting point to determine these values and we apply a Gaussian fit to smooth the distribution. This choice of threshold keeps 50% of the events. This curve represents the peak of the distribution of the beamformer output. This peak is considered as ambient noise.
However, we realize that these threshold choices were too low. We notice that selecting the best one of the 11 starting points what we call optimization brings up a second peak on the distribution (fig. 7a).

The first peaks of the distributions seem to correspond to the noise that cannot be assimilated to any event and is constant. The second peaks of the distributions exists only at low frequency from 5 Hz to 12 Hz, it seems to correspond to signals that would be superimposed and therefore not relocatable. We have deduced that this superposition of signals was probably the result of anthropogenic and hydrological noise which is continuous and existing at low frequency. In this case, we determine a new threshold curve (fig. 7b) after this second peak. The error bars are chosen at one times the variance of the Gaussian fit. We observe that the algorithm has difficulties for fitting around 9 Hz, we explain this by the same importance of both the peak. The new threshold had the effect to increase significantly all the threshold's values for the frequency below 9 Hz. We observe a big step at 9 Hz (fig. 7b) caused by the decrease of the second peak. This effect may be caused by the disappearance of overlapped sources at high frequency.

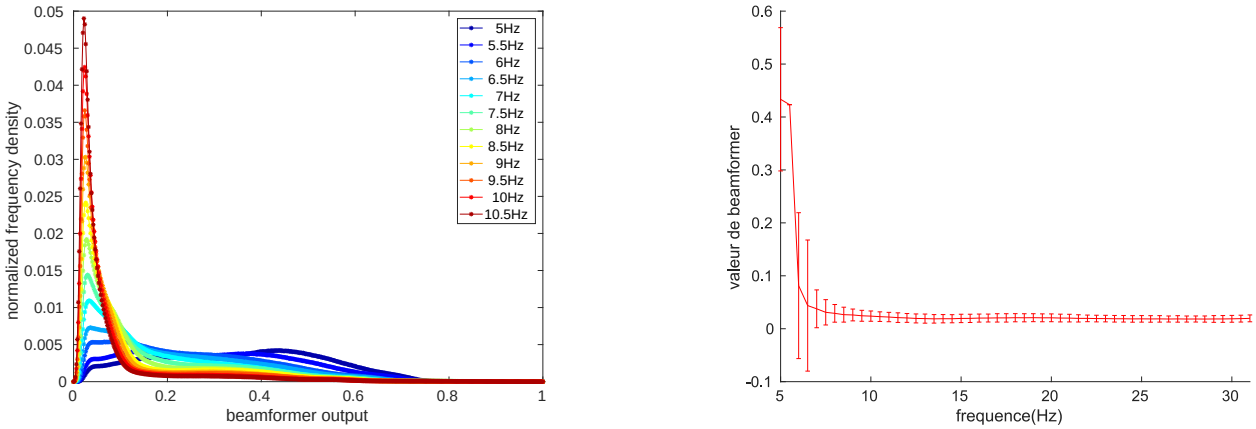

(a) (b)

Figure 6: Distribution of the correlation values for all the frequencies (a) : Distribution of the beamformer output from 5 to 12 Hz (b) : Curve used as the threshold of the highest peak of the distributions of the beamformer outputs for each frequency, fit with a Gaussian. The error bar is one times the variance of the Gaussian.

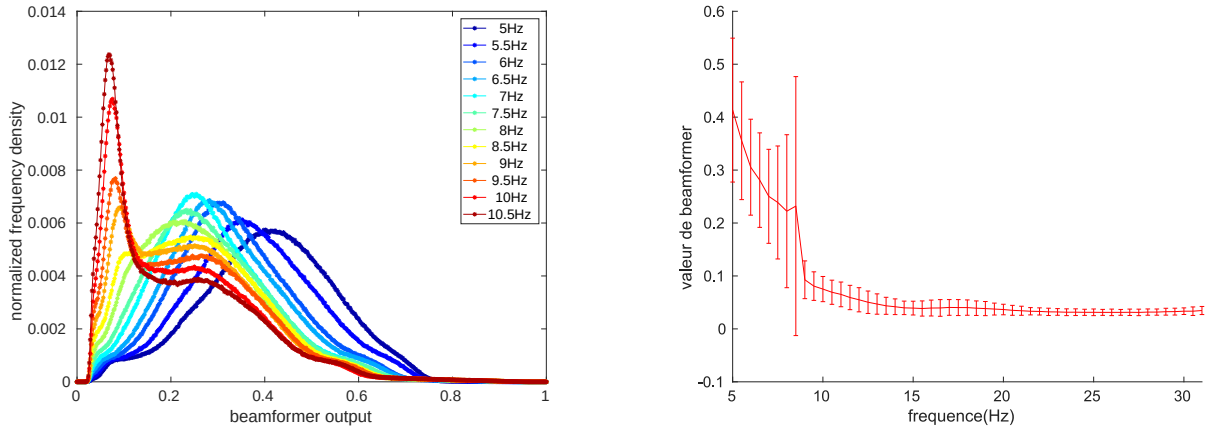

(a) (b)

Figure 7: Distribution of the beamformer output for all the frequencies with optimization on the starting point (a) : Distribution of the beamformer output from 5 to 12 Hz with optimization (b) : Curve used as the threshold of the highest peak of the distributions of the beamformer outputs for each frequency with optimisation, fit with a Gaussian. The error bar is one times the variance of the Gaussian.

In order to characterize the uncertainty and to check the threshold choice done before, we perform the location using a grid search algorithm. This type of algorithm is less efficient but allows to have a notion of uncertainty by a local spot as well as to see local minima. If different sources appear at the same time, we can also observe them. The value of the focal spot is a correlation value of the signals computed for each pixel of the grid. First, we apply the grid search on X and Y-axis, next we choose the higher value of correlation on the Y-axis to choose the X and Z plan where to do the grid search.

If we choose sources with a higher beamformer value, the focal spots shrink significantly and the two methods coincide, as we can see on figure 8a the green and blue circle are close. The comparisons between the maximum of the focal spot and the location by optimization help us to check our threshold values. The interesting part was to see that outside the network the uncertainty values are high,

whatever the value of the beamformer. Although we try to determine a threshold for each frequency in general, we realize that a threshold value is valid for each case.
In figure 8, we present a source located in the network with a really high beamformer output. The focal spot is smaller although the correlation value of the grid search is a bit smaller than for an outside source (fig. 9) while the beamformer output is larger. The size of the focal spot is about 20 meters in the X and Y-axis (fig. 8a) for the best beamformer output. We therefore choose the threshold as soon as the difference between the two methods reaches the size of the horizontal focal spot (20m). The uncertainty inside the mesh is $\frac{\lambda}{2}$ where λ is the wave-length. It is interesting to note this is half the distance between two sensors within the mesh. In the X and Z-axis (fig. 8c), the focal spot is near 200m which is the average thickness of the glacier. The uncertainty is higher in the vertical component due to diffraction, because the node's mesh is set up horizontally.

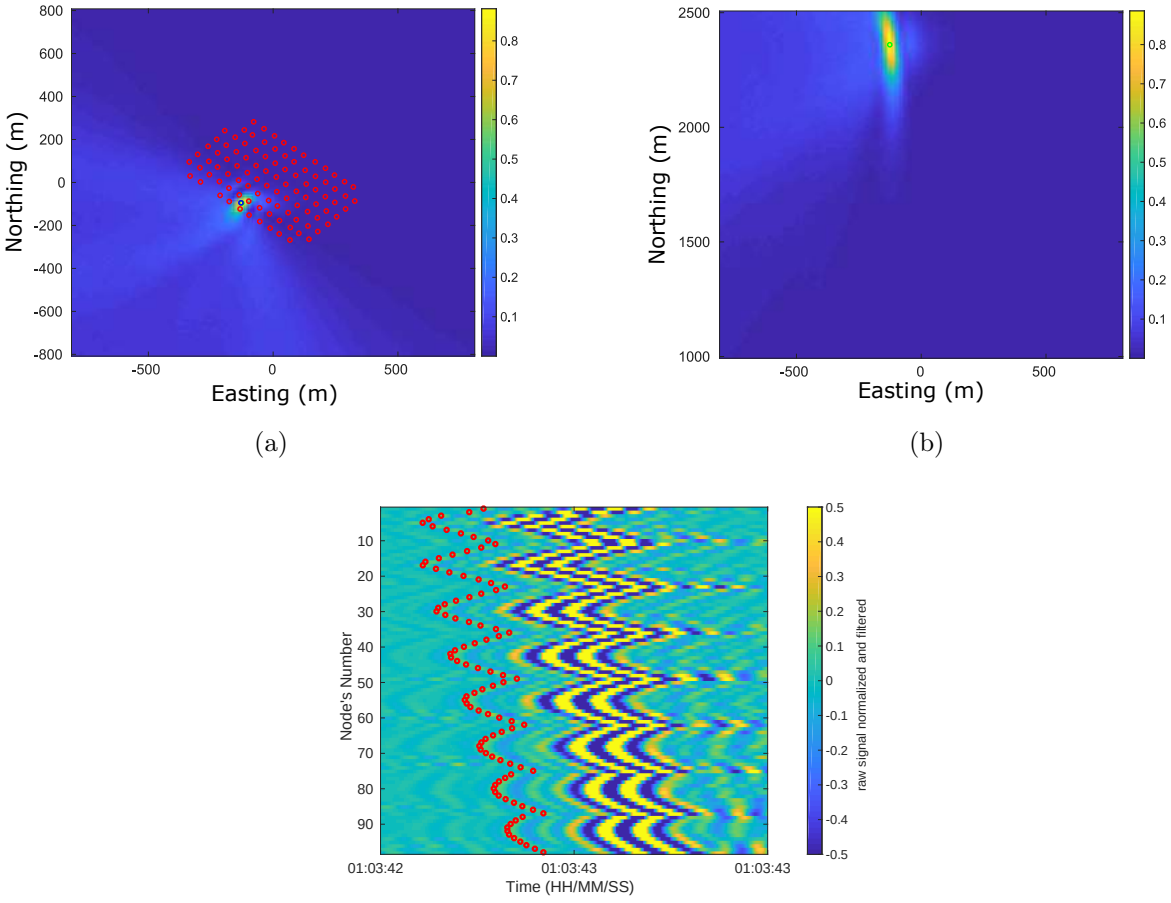

(a) (b) (c)

Figure 8: Uncertainty on inside source location with a good beamformer output $T_B = 0.90397$. (a) : Focal spot of a source located inside the mesh. The red circles are the position of the nodes. The green dot is the location of the source given by the beamformer algorithm. (b) : Focal spot of a source located inside the vertical axis. The green dot is the location of the source given by the beamformer algorithm. (c) : Representation of the raw signal of this source. The red circles are the delays as predicted using the located source inside the mesh

.

For sources outside the network, we will choose to work with azimuths. As we can see in figure 9, a external source to the network gives a very long focal spot of kilometers scale in the X and Y-axis

(fig. 9a) but the correlation value of the grid search is really high, more than 0.8, on a long part of the focal spot. The azimuth of this focal spot is well constrained. The uncertainty outside the mesh is defined by the diffraction law (Chmiel et al., 2019) as $\frac{\lambda F}{D}$ where λ is the wave-length, D is the opening angle and F the frequency.

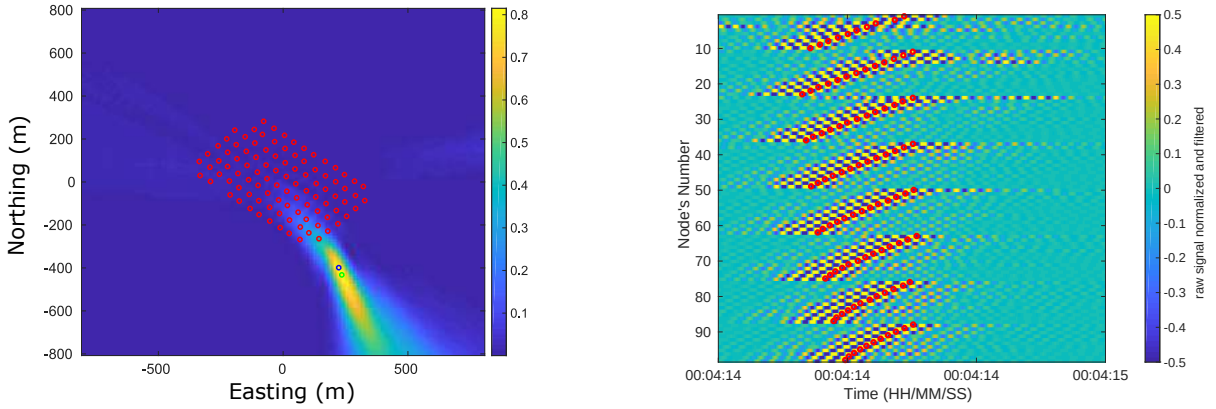

(a) (b)

Figure 9: Uncertainty of a distant source location with a good beamformer output ($T_B = 0.67577$). The red circles are the delay law of the signal. (a) : Focal spot of a distant source located outside of the mesh. The red circles are the position of the nodes. The green dot is the location of the source given by the beamformer algorithm. (b) : Representation of the raw signal of this source. The red circles are the delays as predicted using the located source outside of the mesh.

The comparison between these two methods allows us to observe that low threshold relocations present rather important errors and that several sources (fig. 10a) seem to interfere with each other in the raw signal (fig. 10b). The beamforming and grid search methods point at different sources.

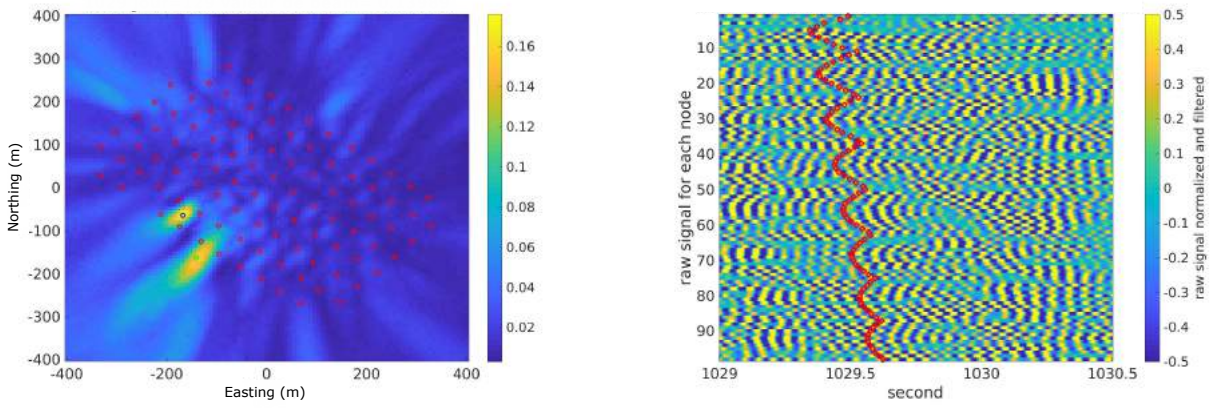

(a) (b)

.

Figure 10: Uncertainty on source location in the mesh with a low beamformer output (Beam=0.13989). The green dot is the location given by the beamformer algorithm. (a) : Focal spots on X and Y-axis of a source located with a low beamformer output. The blue circle is the maximum value of the grid search algorithm. The green circle is the position given by the beamformer. The red circles are the positions of the nodes. (b) : Delay law and raw signal of a source located with a low beamformer output. The red circles are the delays as predicted using the located source inside the mesh

.

To work on the 53-frequency bands, we decide in light of the different observations to choose the highest threshold of the general threshold curve at $T_B = 0,5$. However, when we focus on phenomena such as surface events we apply the threshold defined specifically for the given frequency band.

4 Results

4.1 Overview of the Argentière noise

The sources detected on the glacier are mainly from the surface. The sources are located around the array. We do not detected many sources in the center of the array. Many sources are also located far from the mesh but as shown before the uncertainty on their location is high. On figure 11a, we observe the presence of lots of sources on the left of the glacier. They seem to form curving lines as if they follow the crevasses.
Some sources are located on the cliff outside the glacier and on the moraine. However, we observe some line-shapes near the crevassing part.
The source outside the mesh is badly located and their azimuths provide a good approximation on them. We observe on figure 11b that between 400 and 800m around the mesh, the 2 principle producers of sources seem to be the seracs. The azimuths are showing their orientation.

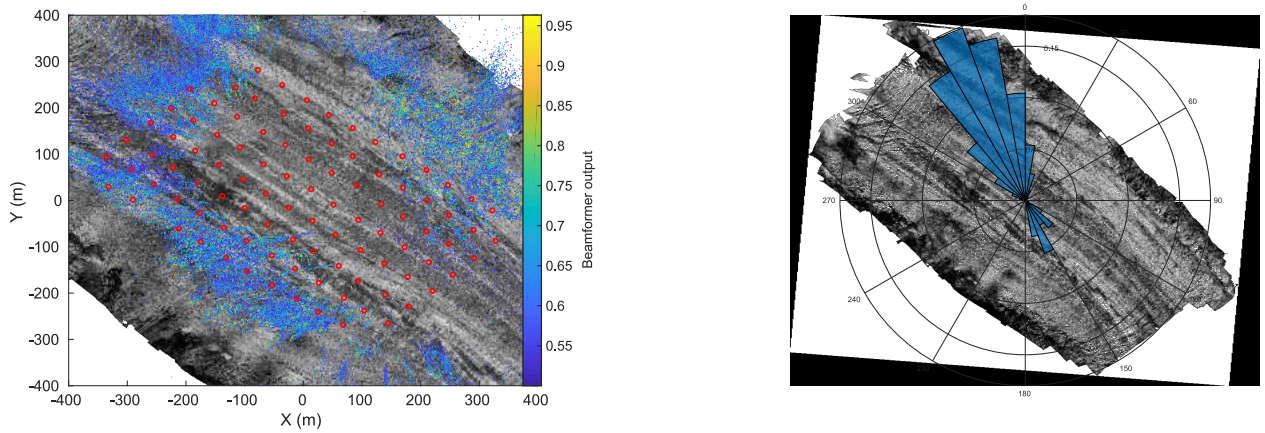

(a) (b)

.

Figure 11: Overview of the source (a) : Map of all the source located at 17Hz during the experimentation with $T_B = 0,5$ and limited to a square of 400m around the center of the mesh. The colors correspond to the value of the beamformer output. (b) : Azimuth of the source outside the mesh between 400 and 800m from the center of the mesh.

Most of the sources observed and located by the MFP are close to the surface. They represent the glacier mechanisms at the surface. They represent the main part of our data set because we can detect them at a wider range of frequencies because of their closest location to the sensor mesh. We isolate these events to determine their proper characteristic.

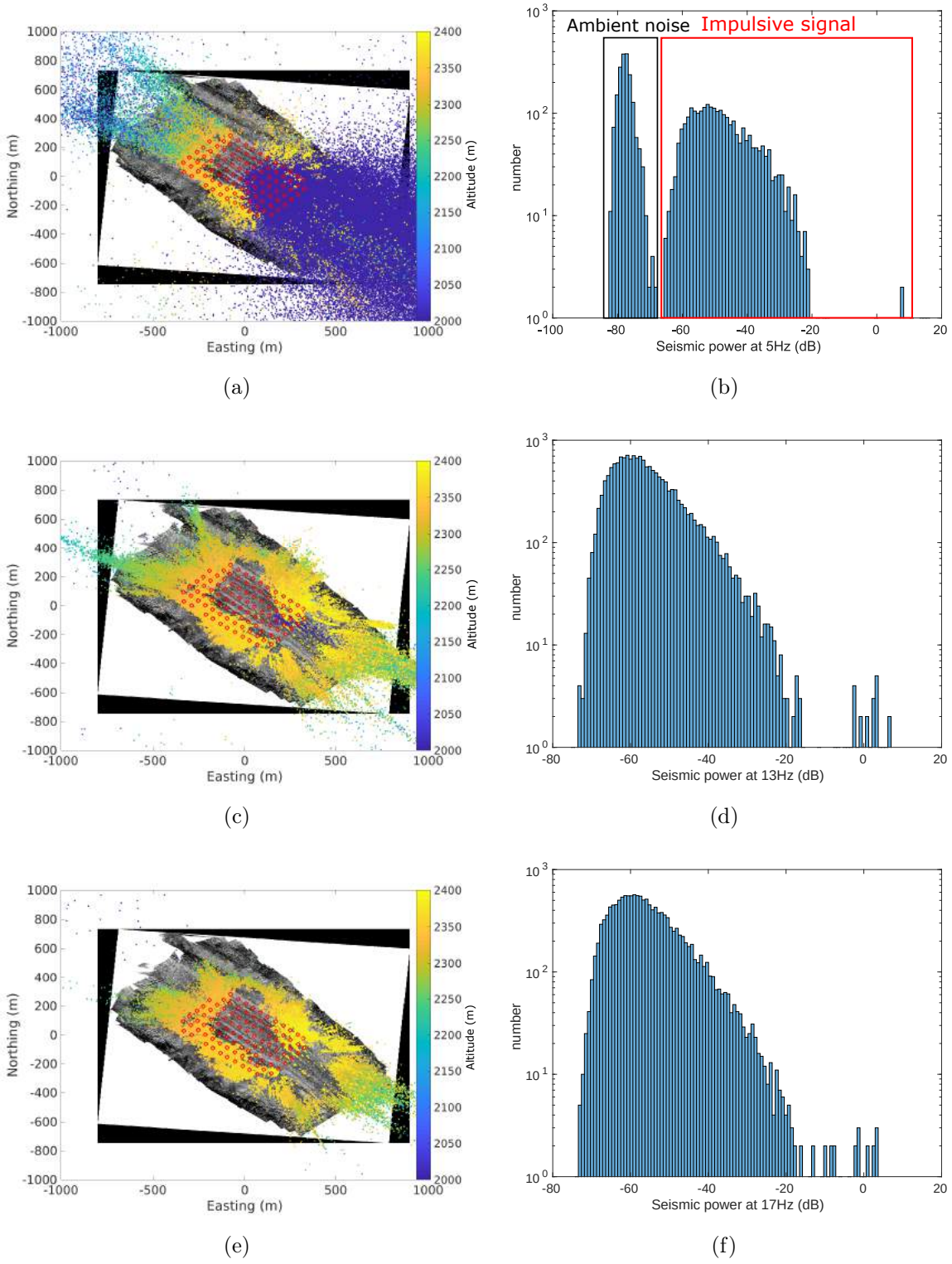

Figure 12: Maps of all the detected sources during the 32 days for a given frequency in a square of one kilometer side centering on the mesh. (a) : 150 317 sources detected at 5Hz (c) : 139 021 sources detected at 13Hz (e) : 101 394 sources detected at 17Hz. The color of the 3 maps correspond to the altitude of the source determined by the beamformer. (b,d,f) show the distribution of energy for a given frequency.

On figure 12, we can observe the variation of the number of sources and their locations as a function of frequency. At 5Hz, figure 12a shows sources at any distance of the mesh and mainly oriented in the axis of the glacier. The distribution of energy (fig. 12b) of these sources shows two different lobes. The

first one from -85 dB to -70 dB seems to be the signature of ambient noise. The second one is wider, from -70 dB to -20 dB, and we find the same shape at 13 Hz (fig. 12d) and 17Hz (fig. 12f). This lobe seems to be linked with the impulsive sources. With the increase of the frequency, the distance sources are closest from the mesh due to the attenuation.
We use 5Hz to observe events from the bed and ambient noise. The frequencies 13Hz and 17Hz are used for the surface events. We do not use intermediate frequencies due to the overlap on frequencies in the beamformer algorithm.

4.2 Sources with energy far above background noise

Here, we look at all the event with an energy content above -70 dB.

4.2.1 The crevasses observed by seismic

The first structure we clearly observe is alignment of sources along the most crevassing parts of the glacier. We observe sources at the same depth in the glacier occurring at the same time or propagating through few hours.

4.2.2 Typical examples of sources around a crevasses

One of the nicest examples is on the second day of the experimentation (fig. 13a). The 25^{th} of April, we observe the propagation during 8 hours from the center of the glacier to the side with 990 sources. A movie of the propagation of the crevasse is visible in the appendix A. It's more than 200 meters long. On figure 13b we clearly observe the beginning of this event at the middle of the day. The seismicity rate per minute of this crevasse seems to be linked with temperature, as we can see on figure 13b. The seismicity rate is the number of events per time step that the beamformer algorithm locate for a defined zone and a define threshold on the beamformer value. The number of source increase after noon with a maximum of 9 events per minutes at 4pm and the temperature is reaching its maximum close to 9°C at 3pm. The sources speed varies between cm/s and a half m/s. We determine a maximum of speed at 2 cm/s (fig. 13c). The sources speed is the velocity of propagation of the sources. It compute between different barycenters of sources by using the mean position and time appearance of the source in the barycenter. The barycenter is created with a radius of 50m and a time step determined for each specific case to provide a better representativeness. The dots' color seems to vary slightly, more greenish with some yellow dots on the left peaks before 10^{-1}m/s and more blueish after, these colors are linked to the color bar of figure 13a.

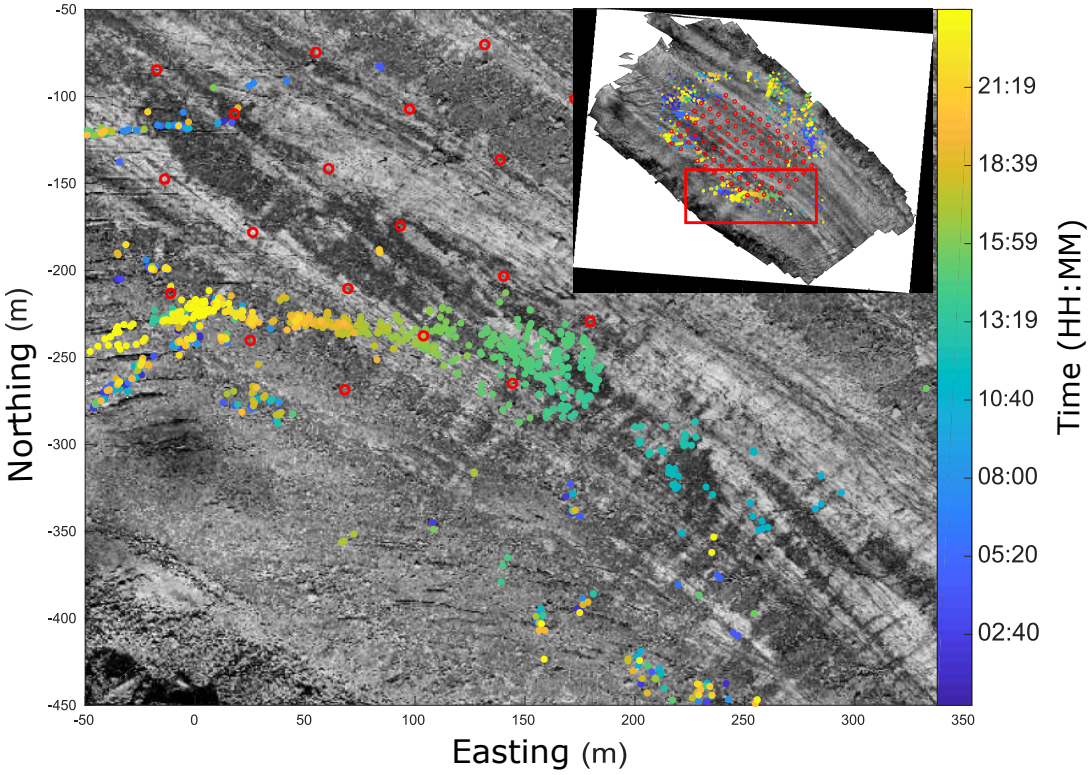

(a)

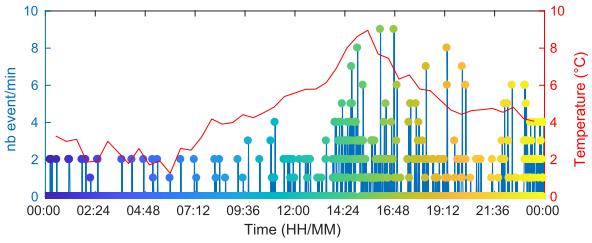

(b)

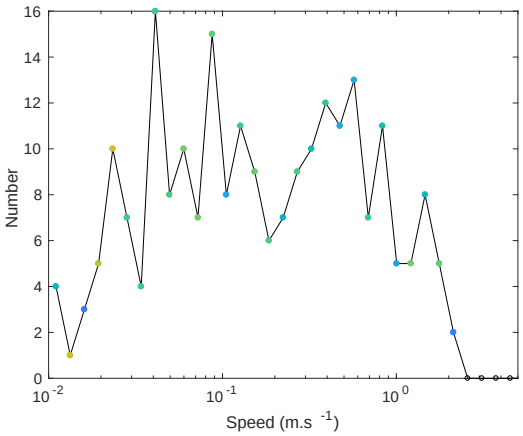

(c)

Figure 13: Examples of sources propagating through a crevasse on the 25^{th} of April. (a) : The points are the source located with the beamformer, their colors correspond to the time during the day. The red circles are the position of the nodes. (b) : seismicity rates observed on the event. The seismicity rates curve is colored by dots as a function of the time. The colors are corresponding to colorbar of (a). (c) : Histogram of the source speed. The colors correspond to the mean time when the speed measurements were done and to colorbar of figure 13a.

The observation made on this example is reproduced on other ones. The source can appear all at the same time or in a really short time scale with a similar shape and number of sources but there are always close to the surface and following the shape of a crevasse. We have differences in some cases.

Figure 14 is another example of sources along a crevasse. The event is propagating during 3 hours. The sources on figure 14a show an expansion of the source line to the left side of the glacier. There

are more blue dots on the right part of this line, but we observe yellow dots on the center and on the left side of this event separated by green's ones. The cracking seems to happen in two places at the same time. The speed of this source is a bit faster than previously exposed, they are around 1m/s(fig. 14b) and the number of speed around the centimeter per second is much lower than previously. We measure speed of more than a meter per second which do not appear in the other examples. The colors of the dots are similar and does not show a variation of speed correlated with the time. The seismicity rate of this short event is pretty high as shown on figure 14c we have 666 events in less than 3 hours.

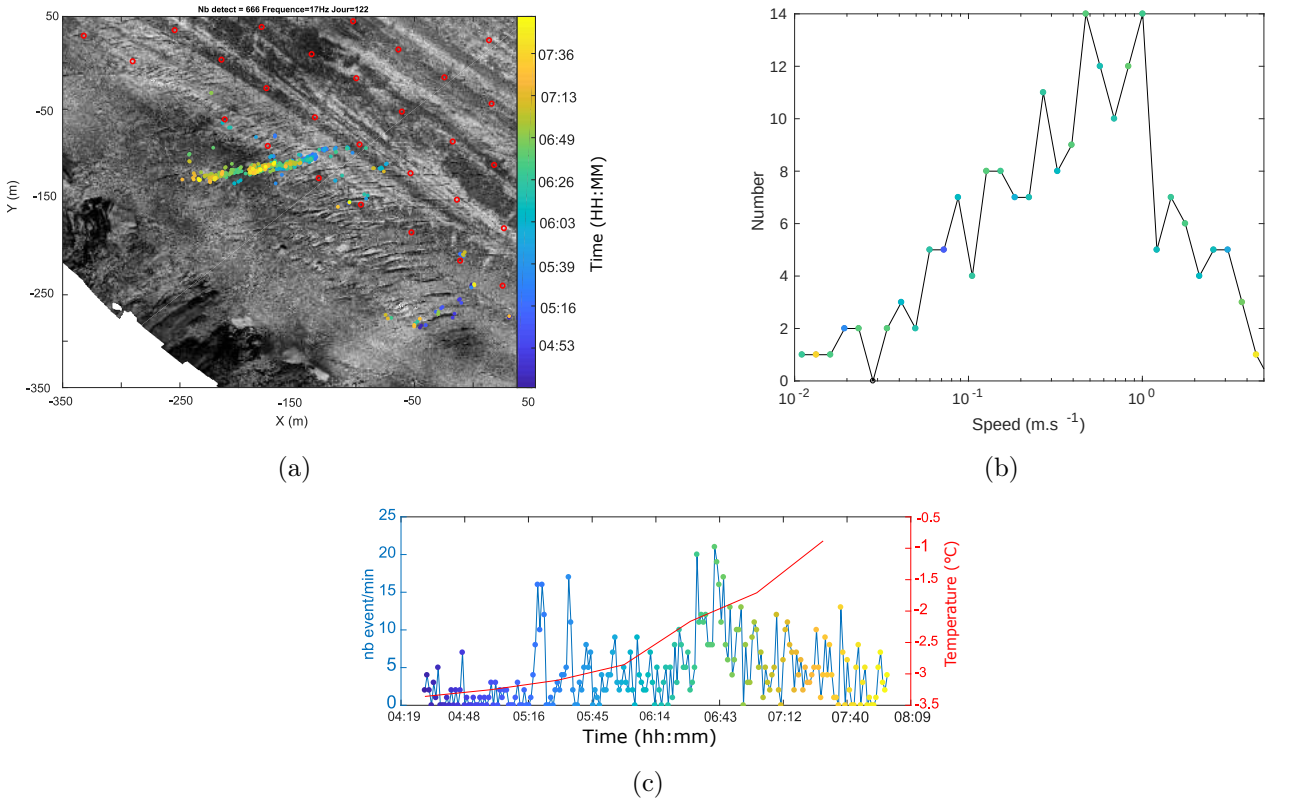

(a) (b)

(c)

Figure 14: Sources following a crevasse on the 1^{st} of May. (a) : The points are the source located with the beamformer, their colors correspond to the time during the day. The red circles are the position of the nodes. (b) : Histogram of the source speed. The colors correspond to the mean time when the speed measurements were done and to the colorbar of figure (a). (c) : seismicity rates observed on the event. The seismicity rates curve is colored by dots as a function of the time. The colors are corresponding to the colorbar of figure (a).

Figure 15 shows the details of different propagating sources. We observed on figure 15a that there are at least 3 events in this area during the day 130 with 1072 sources. The different events are visible on the seismicity rates of the area (fig. 15d). We have a first increase of events at 8am, the next one is at 2pm and the last significant one at 10pm. The first one seems to appear during an important variation of temperature and the last one too. The number of events is not related to temperature here. Figure 15c details the speed of source propagation during the whole day, which is around the cm/s. The color of the dots are more greenish below 10^{-1}m/s and after a bit more blueish. If we select the last event of the day, figure 15b shows the propagation of sources from the center to the side with a time scale shorter than observed above.

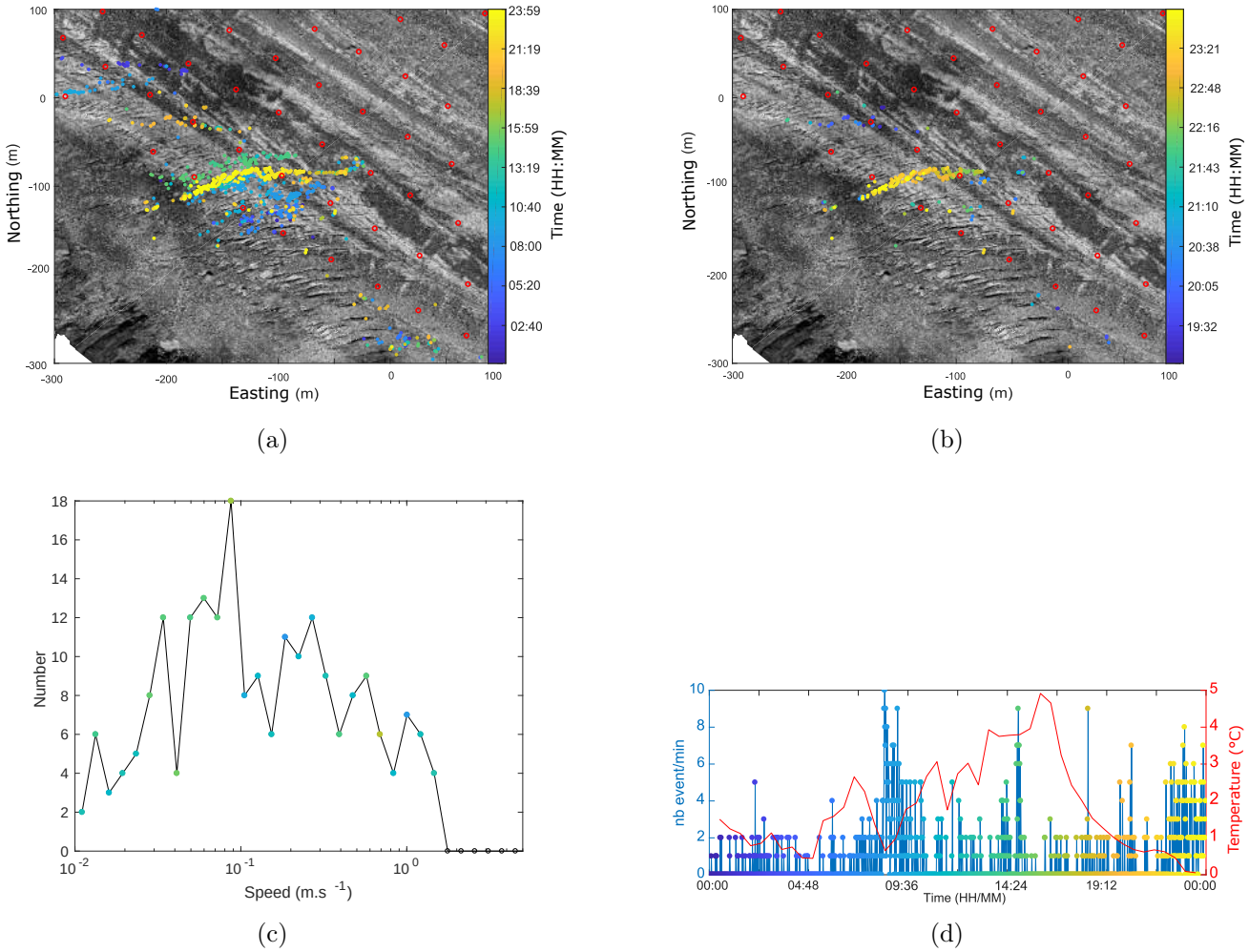

Figure 15: Crevasses located on the 9^{th} of May (a) : Map showing groups of sources along different crevasses. The points are the source located with the beamformer, their colors correspond to the time during the day. The red circles are the position of the nodes. (b) : Selection of a shorter time interval to observe the propagation of the source from the center to the side. The points are the source located with the beamformer, their color corresponds to the time during the day. The red circles are the position of the nodes. (c) : Histogram of the source speed. The colors correspond to the mean time when the speed measurements were done and to the colorbar of (a). (d) : seismicity rates observed on the event. The seismicity rates curve is colored by dots as a function of the time. The colors are corresponding to figure (a)

.

4.2.3 Seismicity rates and temperature variation

The seismicity rates on the whole mesh show daily variations and when we compare them to temperatures. They seem to be linked with low temperatures (fig. 16). These results surprise but were also already observed in Podolskiy et al. (2018) and explained as thermal cracking.

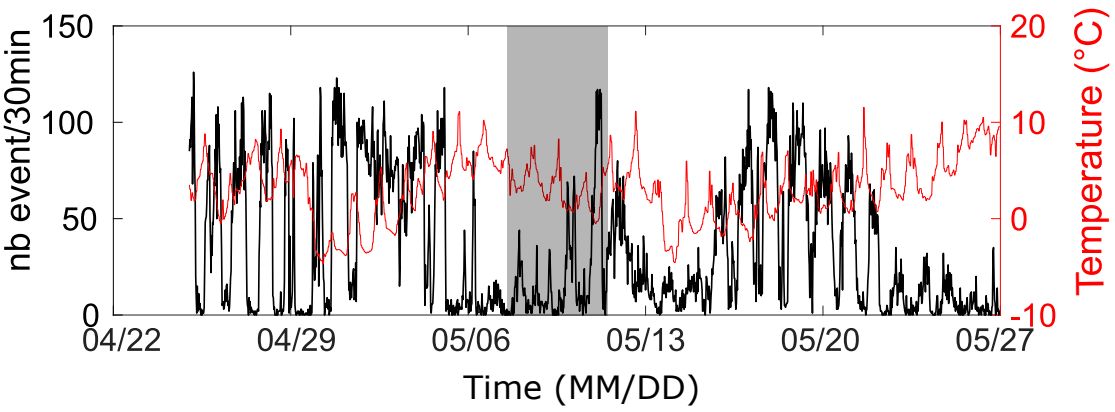

Figure 16: seismicity rates inside the mesh during the whole experimentation with $T_B = 0.5$ at 5Hzcompared to the temperature. The gray area is a period when some nodes were on the side and switch off.

This variation of seismicity rates can also be an artifact of a bigger ambient noise. The ambient noise can be too strong during the day and able to hide some sources. It contributes to a diminishing of the number of well located sources because the beamformer can locate only a source per time window. The results with a higher threshold on the beamformer output show similar results on figure 17. We have to stay cautious because the number of events is much lower, we had to change the frequency to have enough significant events. We count very few events, often less than 20 per half-hour but they have a really good phase coherence and no noise on the signal. We also observe the absence of events from the 8 to 12^{th} of may, the gray area on figure 16 and 17. We explain it by sensors failover due to the snow melting. With less sensors, the phase coherence is decreasing and this explains a total absence of sources above $T_B = 0.8$. It may also be the reason why on figure 16 we have fewer events in the gray area.

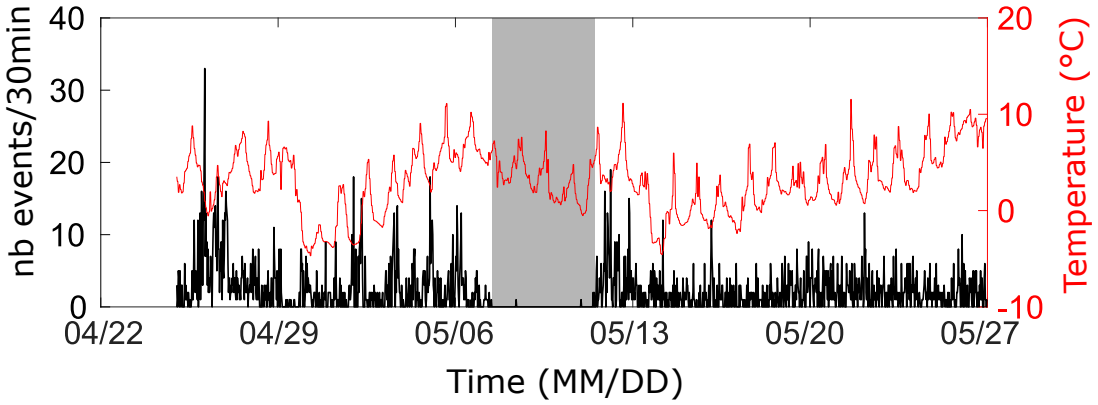

Figure 17: seismicity rates inside the mesh during the whole experimentation with a high threshold $T_B = 0.8$ at 13Hz compared to the temperature. The gray area is a period when some nodes were on the side and switch off.

Only the energy of the event can confirm these assumptions. We would like to confirm that the variation of energy are similar to the variation of seismicity. The energy of events, the ones used to calculate the seismicity rates in figure 16, does not show a clear result. Main of the spike seems to appear just before the temperature peak (fig. 18). If we compare to the noise energy, the event energy is much higher, meaning there is not artifacts from the noise. Only at the end of April the noise is

much higher and may interfere with the location of the event.

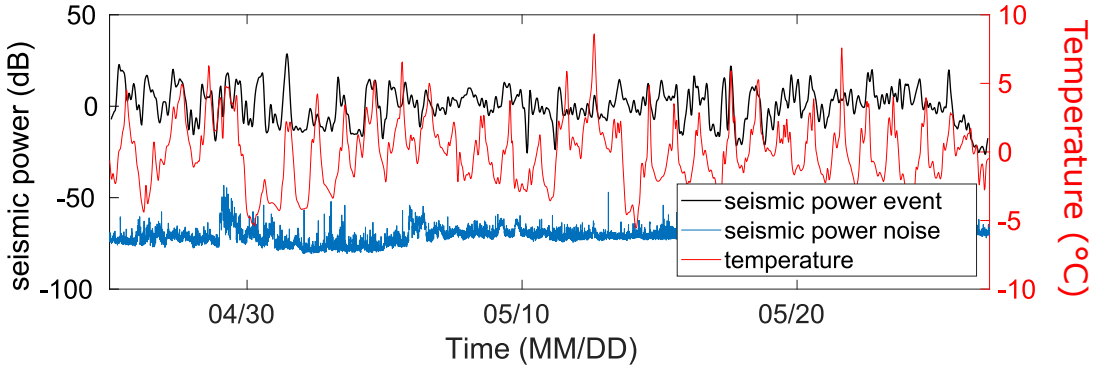

Figure 18: Energy of the events used in the seismicity rates in black. The red curve is the temperature and the blue one is the ambient noise.

If we look at a "mean day" (fig. 19) by doing the means of every variable for the 32 days we obtain a peak of energy before the peak of temperature. The noise does not present daily variation. The seismicity rate on the mesh is high during the night and low during the day.

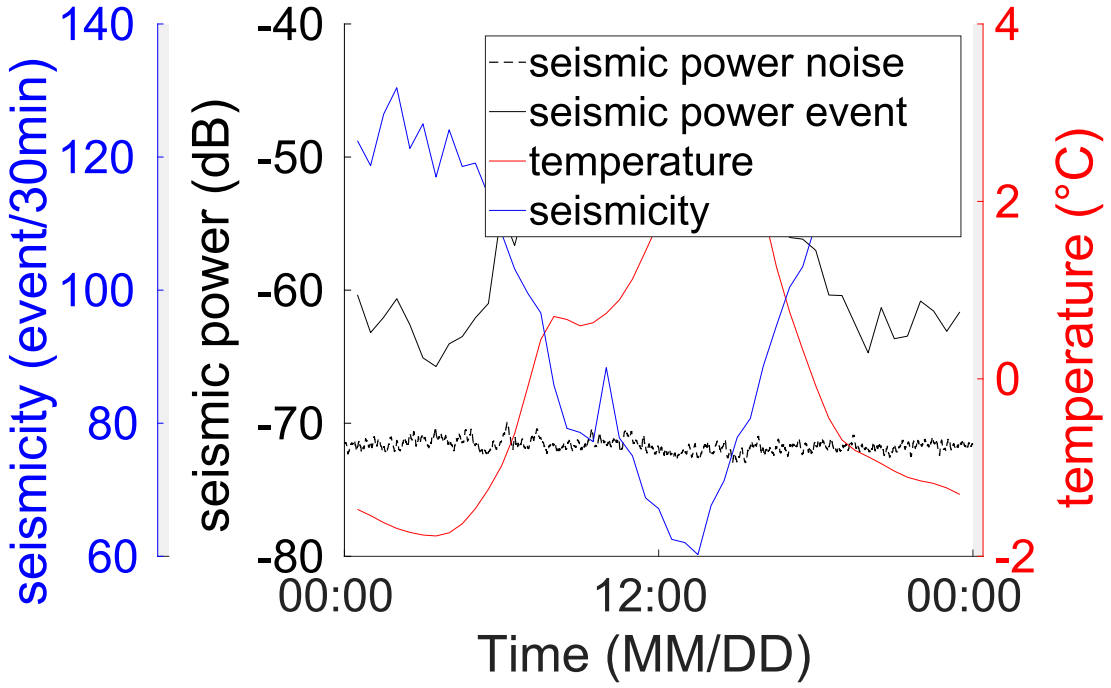

Figure 19: Mean day of the seismic power of noise, the temperature and the seismic power of events

4.2.4 Distribution of energy

Here we look at the distribution of seismic power associated with impulsive events in the idea of characterizing a proxy of the so-called Gutenberg-Richter law for earth. This law describes the number of earthquakes per time unit at a given energy. In the case of a glacier, it's not common to calculate

this distribution which is similar to the Gutenberg-Richter law because we did not have enough sources with a well defined energy and location.
The variation of the law is related to the media. We observe on figure 20, the distribution of energy for 3 frequencies, 5, 13 and 17 Hz. We fit a power law on the first 20 bins. At 5Hz (fig. 20a), the slope is much lower than with higher frequency. The slope differences between the night and the day are not strong but enough to be significant with the logarithm scale.

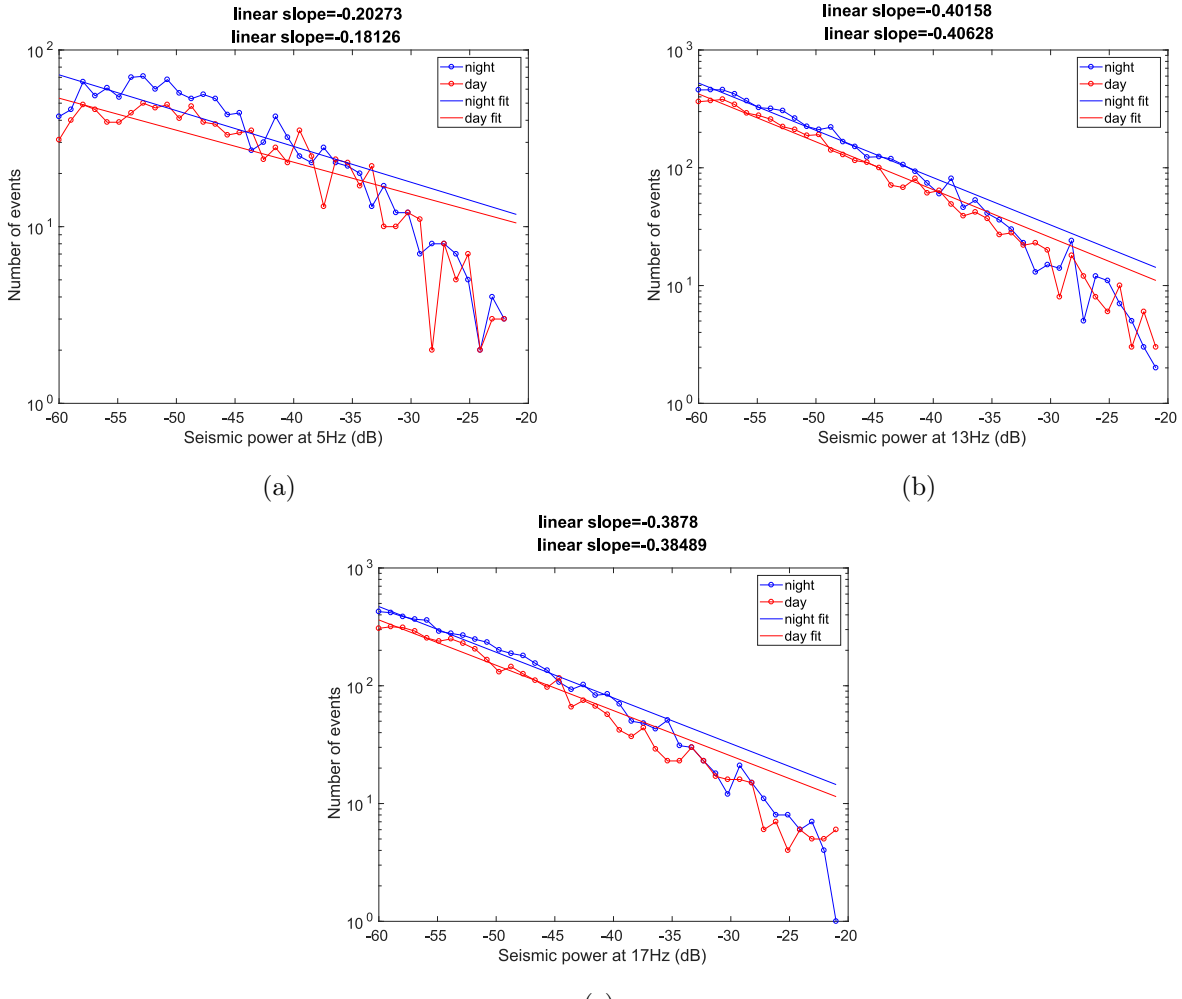

Figure 20: Distribution of energy of the source at a given frequency on the mesh area. (a) : 5Hz (b) : 13Hz (c): 17Hz

4.2.5 rockfalls

The glacier is covered by snow but also by rocks. They come from the cliff and moraines.The sun is realizing the rock from their enclosure of snow and ice which are falling on the glacier. The effect of the sun is stronger on the steepest and southern slopes.
We think we have found the signature of these events on our seismic records. It looks like nuclei of sources on some area. We observe especially at the border between the glacier and the moraine a nucleus which occur at least every days. When we look on the drone picture of this area, it's looking to be a common place for rock falling. The rocks are forming a scree there. They may fall from the moraine to the glacier and cover the border. It is probable that these rocks are producing seismic sources. We mainly make this observation at the bottom of the south face of the mountain, more

impacted by the sun and the temperature. It's not surprising to found a link with the temperature and this seismic source.

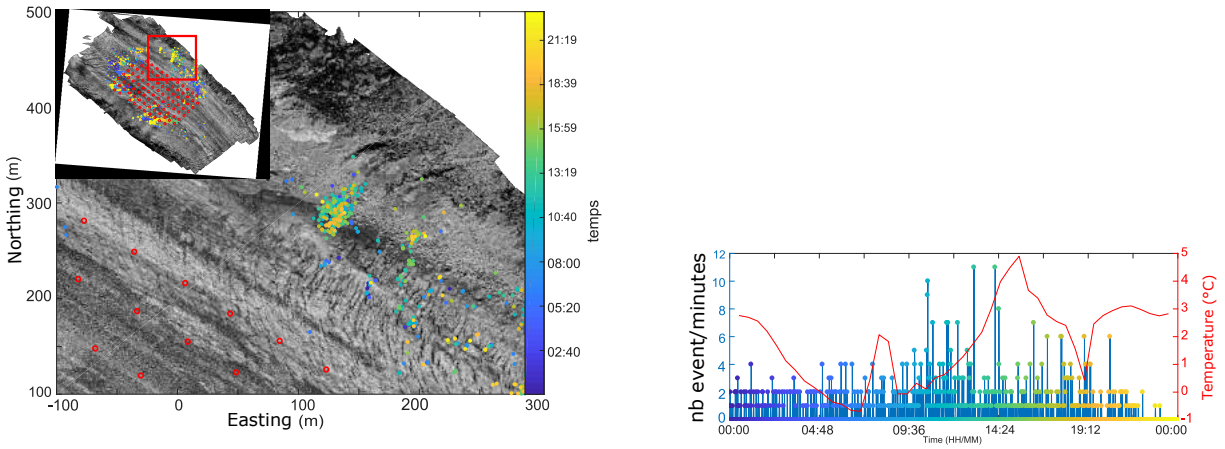

(a) (b)

Figure 21: rockfalls on the glacier recorded with seismic sensors (a) : Map showing rockfalls located on the glacier(b) : seismicity rates of the rock fall area. The color dots correspond to the colorbar of (a).

4.3 Sources with energy close to the background noise

4.3.1 Within the array

The ambient noise is also coming from the array. The raw signal show on figure 22 we observe a phase coherence which confirm the output value of the beamformer higher than 0,6 but the beamformer compute a too low time delay if we compare to the signal phase. The localisation computed by the beamformer will surely be wrong.

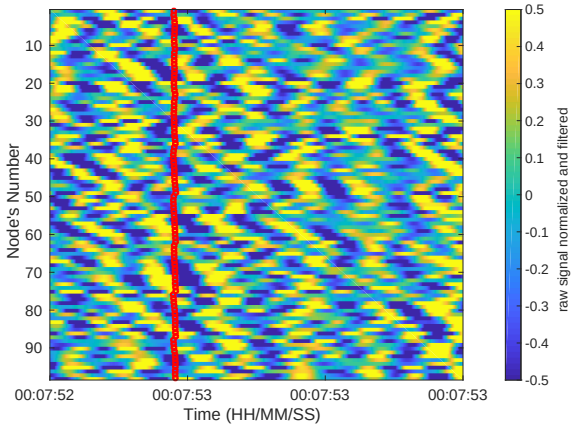

Figure 22: Raw signal of one of the sources located inside the mesh and with an energy lower than -70 dB. The red circles are the delays as predicted using the located source inside the mesh.

However, the seismicity rate of these low energy events is interesting. On figure 23, we observe a diurnal variations link to the temperature in opposition of phases. The water discharge is correlated with appearing of peaks of seismicity rates. When the water discharge increase from the 6^{th} to the 15^{th}

of May, we observe an increase of the seismicity rates which is following the water discharge variation. The variation of the seismicity rates seem to be in coherence with the temperature and the water discharge.

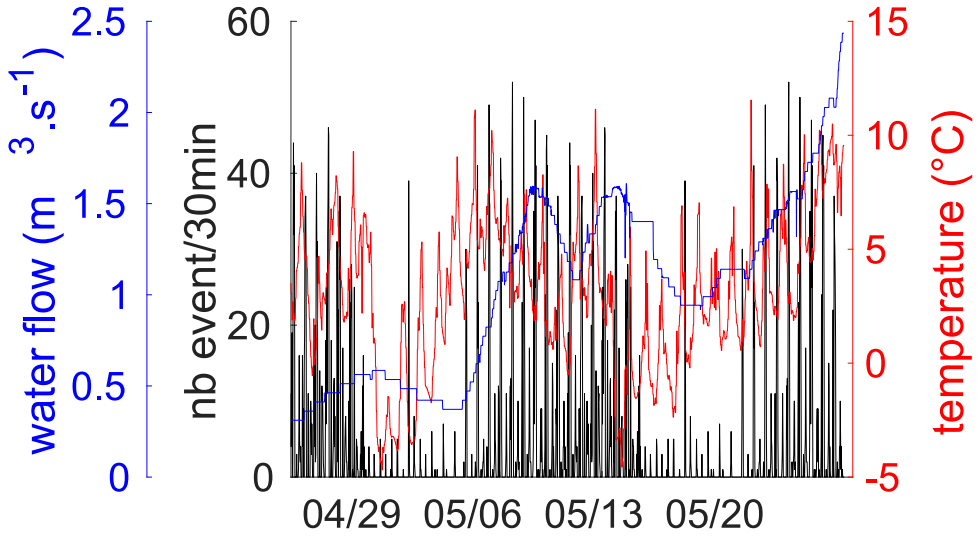

Figure 23: Seismicity rates for events below -70 dB and located inside the mesh. The red curve is the temperature and the blue one the water discharge

4.3.2 Anthropogenic and outside of the array noise

As we establish before the uncertainty outside the mesh is really high and it's increasing with the distance. However we try to take a short look at the far source to have information on the anthropogenic noise. These sources are mainly detected at low frequencies around 5Hz. We choose to use only the azimuth of the sources due to the uncertainties of the location at this distance. On figure 24, we can see the event at 5Hz and more than 8 km. The azimuth of these events is indicated the Emosson barrage where the water from Argentière is driving and also seems to indicate the valley of Martini. It's weird to have noise from this valley and not from Chamonix valley. There are more than 50 000 sources on these azimuths which give a significant weight to this result.

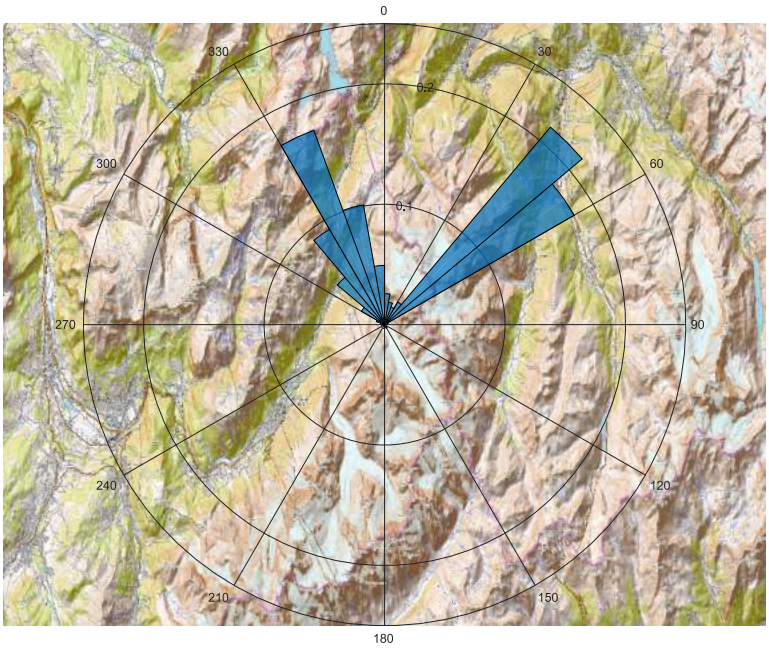

Figure 24: Events further than 8000m from the mesh

4.4 The surface waves dispersion curve and inversion of the glacier structure

A velocity versus frequency dispersion curve (fig. 25) has been done by a statistical way which is not common. We made the distribution of the sources "well" located as a function of the speed propagation compute by the beamformer for each frequency and took the highest value to have the curve. It may be inverted to obtain the thickness of the constitution of the media. With the velocity variation as a function of frequency, we obtain the depth of the boundary by trying different possible models. In our case, we would like to have the ice thickness of the glacier under the mesh so the data was selected to be located in the mesh and at a depth corresponding to the glacier. The problem with this method is the more we want to look deeper and more our dispersion curve has to go to low frequency.

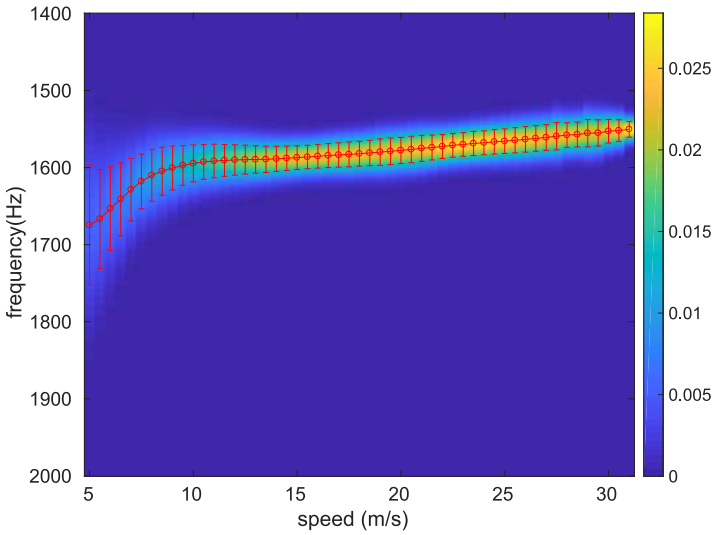

Figure 25: Distribution of the propagation velocity values for all the frequencies fit with a Gaussian. The red curve is the maximum value for each frequency. The error bars are one times the variance.

Thanks to Stéphane Garambois (ISTerre) and the software geopsy, we perform an inversion of the dispersion curve. The software is fitting different models to found the one corresponding to the dispersion curve(fig. 26a) and the different models correspond to a two layers media with a define density and range of velocity propagation. However, the models have defined the rock / ice interface at 150m (fig. 26b) which is too weak for this place of the glacier. This may be due to a lack of information in the low frequencies.

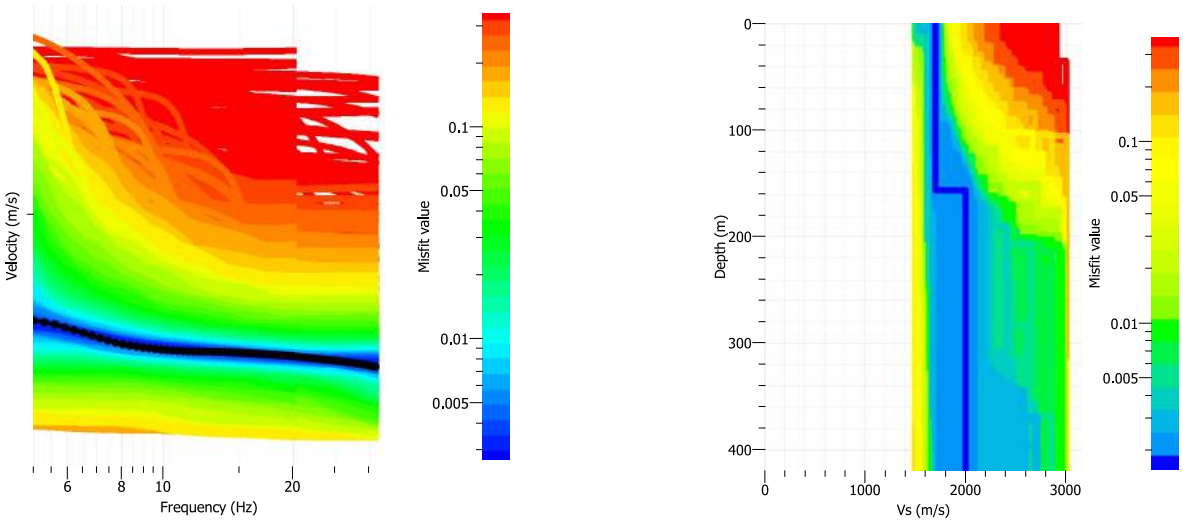

(a) (b)

Figure 26: Model outputs from geopsy (a) : Distribution of the velocity versus frequency modeled by geopsy. The colorbar corresponds to the misfit between the model and the given dispersion curve. (b) : Distribution of the velocity versus depth modeled by geopsy. The colorbar corresponds to the misfit of the model.

5 Discussion

Our algorithm did the location without distinguishing the source type (continuous or impulsive). We determine to have the source with a good coherence of phase T_B have to be at 0,5 meaning we are taking sources above the noise where is contained the continuous sources. It was not the goal in our case but to have only good location we select impulsive sources. It can be relevant to use a different method to identify continuous sources from hydrological noise.

The results show propagation of sources on the surface of the glacier along crevasses. We understand that the displacement speed of theses sources is too fast to be linked with the glacier sliding. It seems the sources speed too low to be fracturing in the ice as it's already known, in Weiss (2004) they define the crack propagation speed close to the speed of body waves ($\approx$ 3300m/s). In this study, they explain cases of slower propagation of cracking or crevasse propagation observed by satellite on the ice-shelves. They observed propagation of several mm/swhich can correspond to the observation made on Argentière. The dynamic of ice-shelves is different and it is difficult to compare events with those on mountain glaciers which have different and continuous constraints. This event is not always correlated with the temperature, they also occur during the night and maybe due to the glacier movement when the flow pass from ductile to fragile mechanism. On other important fact is that the sources along crevasses are always propagating from the center to the side of the glacier. The glacier velocity is higher in the center part and the friction on the side reduce the velocity which creates these crevasses area and can explain this propagation line.

The seismic activity on the glacier seems to be linked with the variation of temperature. The variations of temperature are producing impulsive sources because there are still observable at high T_B. When we look to the energy the variation is shifted. We understand this by the increasing of events at the highest variation of temperature and the event are more energetic before the peak of temperature. These impulsive sources seem to be related to crevasse activity as the main observed sources.

The link with the temperature does not direct some other mechanisms seems to be involved explaining it. A direct link with daily variation of temperature is not possible because the glacier was recovered of more than 2 meters of snow during a long part of the experimentation. Gilbert et al. (2014) shows that the daily variation of temperature only impact the first half meter in the best condition in the case of dry snow. During this period of the year, the melting is at its highest point and the snow is saturated in water so is temperature is constant at 0°C (Fierz et al., 2009). The melt water start to flow in the crevasses and seracs.

The events below -70 dB inside the mesh are badly relocated by the beamformer. Their locations are too deep with a bad definition of the time delay. However, they are presenting coherence with the temperature and the water discharge which imply the sources are certainly on the glacier. They could be really interesting to use another method to process this precise data.

6 Conclusion

This dissertation has investigated the usefulness of a seismic array on a glacier. The results are really promising. In this investigation, the aim was to apply a seismic dense array on a glacier to have a better understanding of its physical mechanisms. The use of the beamformer to locate sources permits a great number and a diversity of types of location. The number of sources provided by the method was impressive if we compare to previous study.

The visualization of the crevasses with seismicity rates is pretty relevant. It provides notions of seismicity rates and propagation of the crack. Their connection with temperature is evident for some of the cases but the linked is not direct. The way to propagate is defined by the sliding of the glacier. The cracking starts from the center and propagates to the side. The results on the propagation speed suggest we observe the formation of cracking or crevasse formation and we are able to define their velocity.

With a wide view, the seismicity rates seem to be linked with the low temperatures. However, it is obvious that other processes are occurring. This explains the relative link between these parameters. The observations show that a large number of events does not signify a high energy for these events.

The current study was limited by the absence of detection of continuous events which occur with hydrology or at the base of the glacier. This effect is caused by the method which has a good phase coherence on impulsive signals. A use of a different method as Agnès Helmstetter do, provide better results on the stick-slip events. The results also show sources from outside as rockfall and anthropogenic noise.

The data still need lots of explorations on them. We only used little part of what we expect they provide. Time needs to be spent on them, and the future results from project SAUSSURE will complete the data set of Argentière and help to explain the observations. Different methods are currently used on the same raw data by Agnès Helmstetter and Ugo Nanni, they focus respectively on the stick-slip events and the subglacial hydrology and channel formation.

References

Aster, R. and Winberry, J.: Glacial seismology, Reports on Progress in Physics, 80, 126 801, 2017.

Bamber, J. L., Westaway, R. M., Marzeion, B., and Wouters, B.: The land ice contribution to sea level during the satellite era, Environmental Research Letters, 13, 063 008, 2018.

Chmiel, M., Roux, P., and Bardainne, T.: High-sensitivity microseismic monitoring : Automatic detection and localization using matched-field processing and dense patch array, under revision, 2019.

Colgan, W., Rajaram, H., Abdalati, W., McCutchan, C., Mottram, R., Moussavi, M. S., and Grigsby, S.: Glacier crevasses: Observations, models, and mass balance implications, Reviews of Geophysics, 54, 119–161, 2016.

Fierz, C., Armstrong, R. L., Durand, Y., Etchevers, P., Greene, E., McClung, D. M., Nishimura, K., Satyawali, P. K., and Sokratov, S. A.: TheInternational Classificationi for Seasonal Snow on the Groun, vol. 5, UNESCO/IHP, 2009.

Fountain, A. G. and Walder, J. S.: Water flow through temperate glaciers, Reviews of Geophysics, 36, 299–328, 1998.

Gerbaux, M., Genthon, C., Etchevers, P., Vincent, C., and Dedieu, J.: Surface mass balance of glaciers in the French Alps: distributed modeling and sensitivity to climate change, Journal of Glaciology, 51, 561–572, 2005.

Gilbert, A., Vincent, C., Six, D., Wagnon, P., Piard, L., and Ginot, P.: Modeling near-surface firn temperature in a cold accumulation zone (Col du Dôme, French Alps): from a physical to a semi-parameterized approach, The Cryosphere, 8, 689–703, 2014.

Gimbert, F., Tsai, V. C., and Lamb, M. P.: A physical model for seismic noise generation by turbulent flow in rivers, Journal of Geophysical Research: Earth Surface, 119, 2209–2238, 2014.

Gimbert, F., Tsai, V. C., Amundson, J. M., Bartholomaus, T. C., and Walter, J. I.: Subseasonal changes observed in subglacial channel pressure, size, and sediment transport, Geophysical Research Letters, 43, 3786–3794, 2016.

Gradon, C., Moreau, L., Roux, P., and Ben Zion, Y.: Analysis of surface and seismic sources in dense array data with Match Field Processig and Markov Chain Monte Carlo sampling, in Press, 2019.

Helmstetter, A., Nicolas, B., Comon, P., and Gay, M.: Basal icequakes recorded beneath an Alpine glacier (Glacier d'Argentière, Mont Blanc, France): Evidence for stick-slip motion?, Journal of Geophysical Research: Earth Surface, 120, 379–401, 2015.

Huss, M., Zemp, M., Joerg, P. C., and Salzmann, N.: High uncertainty in 21st century runoff projections from glacierized basins, Journal of Hydrology, 510, 35–48, 2014.

Larose, E., Carrière, S., Voisin, C., Bottelin, P., Baillet, L., Guéguen, P., Walter, F., Jongmans, D., Guillier, B., Garambois, S., et al.: Environmental seismology: What can we learn on earth surface processes with ambient noise?, Journal of Applied Geophysics, 116, 62–74, 2015.

Pepin, N., Bradley, R., Diaz, H., Baraër, M., Caceres, E., Forsythe, N., Fowler, H., Greenwood, G., Hashmi, M., Liu, X., et al.: Elevation-dependent warming in mountain regions of the world, Nature Climate Change, 5, 424, 2015.

Podolskiy, E. A. and Walter, F.: Cryoseismology, Reviews of geophysics, 54, 708–758, 2016.

Podolskiy, E. A., Fujita, K., Sunako, S., Tsushima, A., and Kayastha, R. B.: Nocturnal thermal fracturing of a Himalayan debris-covered glacier revealed by ambient seismic noise, Geophysical Research Letters, 45, 9699–9709, 2018.

Preiswerk, L. E. and Walter, F.: High-Frequency (> 2 Hz) Ambient Seismic Noise on High-Melt Glaciers: Green's Function Estimation and Source Characterization, Journal of Geophysical Research: Earth Surface, 123, 1667–1681, 2018.

Preiswerk, L. E., Michel, C., Walter, F., and Fäh, D.: Effects of geometry on the seismic wavefield of Alpine glaciers, Annals of Glaciology, pp. 1–13, 2018.

Rabatel, A., Dedieu, J.-P., and Vincent, C.: Using remote-sensing data to determine equilibrium-line altitude and mass-balance time series: validation on three French glaciers, 1994–2002, Journal of Glaciology, 51, 539–546, 2005.

Rabatel, A., Sanchez, O., Vincent, C., and Six, D.: Estimation of glacier thickness from surface mass balance and ice flow velocities: a case study on Argentière Glacier, France, Frontiers in Earth Science, 6, 112, 2018.

RESOLVE: WP1 - Geophysical investigation of the Argentière Glacier (Chamonix Valley, French Alps), URL `https://resolve.osug.fr/spip.php?rubrique10`, 2017.

Richardson, J. P., Waite, G. P., FitzGerald, K. A., and Pennington, W. D.: Characteristics of seismic and acoustic signals produced by calving, Bering Glacier, Alaska, Geophysical Research Letters, 37, 2010.

Sergeant, A., Mangeney, A., Yastrebov, V. A., Walter, F., Montagner, J.-P., Castelnau, O., Stutzmann, E., Bonnet, P., Ralaiarisoa, V. J.-L., Bevan, S., et al.: Monitoring Greenland ice sheet buoyancy-driven calving discharge using glacial earthquakes, Annals of Glaciology, pp. 1–21, 2019.

Soruco, A., Vincent, C., Rabatel, A., Francou, B., Thibert, E., Sicart, J. E., and Condom, T.: Contribution of glacier runoff to water resources of La Paz city, Bolivia (16 S), Annals of Glaciology, 56, 147–154, 2015.

Vaughan, D. G., Comiso, J. C., Allison, I., Carrasco, J., Kaser, G., Kwok, R., Mote, P., Murray, T., Paul, F., Ren, J., et al.: Observations: cryosphere, Climate change, 2103, 367, 2013.

Vincent, C. and Moreau, L.: Sliding velocity fluctuations and subglacial hydrology over the last two decades on Argentière glacier, Mont Blanc area, Journal of Glaciology, 62, 805–815, 2016.

Vincent, C., Soruco, A., Six, D., and Le Meur, E.: Glacier thickening and decay analysis from 50 years of glaciological observations performed on Glacier d'Argentière, Mont Blanc area, France, Annals of glaciology, 50, 73–79, 2009.

Vincent, C., Garambois, S., Thibert, E., Lefebvre, E., Le Meur, E., and Six, D.: Origin of the outburst flood from Glacier de Tête Rousse in 1892 (Mont Blanc area, France), Journal of Glaciology, 56, 688–698, 2010.

Vincent, C., Descloitres, M., Garambois, S., Legchenko, A., Guyard, H., and Gilbert, A.: Detection of a subglacial lake in Glacier de Tête Rousse (Mont Blanc area, France), Journal of Glaciology, 58, 866–878, 2012.

Vivian, R. and Bocquet, G.: Subglacial cavitation phenomena under the glacier d'Argentière, Mont Blanc, France, Journal of Glaciology, 12, 439–451, 1973.

Walter, F., Canassy, P. D., Husen, S., and Clinton, J. F.: Deep icequakes: What happens at the base of Alpine glaciers?, Journal of Geophysical Research: Earth Surface, 118, 1720–1728, 2013.

Weiss, J.: Subcritical crack propagation as a mechanism of crevasse formation and iceberg calving, Journal of Glaciology, 50, 109–115, 2004.

List of Figures

A Movie of the crevasse present on figure 13

https://youtu.be/aPm-7r3EKDk